Metamaterial sandwich plates with two-degree of freedom inertial amplified resonators for broadband low-frequency vibration attenuation

Lei Gao [a], Cheuk Ming Mak [a] *, Chenzhi Cai [b] and Supeng Deng [a]

[a] *Department of Building Environment and Energy Engineering, The Hong Kong Polytechnic University, Hung Hom, Kowloon, Hong Kong*

[b] *School of Civil Engineering, Central South University, Changsha, Hunan, China*

*Corresponding author.
E-mail Address: cheuk-ming.mak@polyu.edu.hk
Telephone: +852 2766 5856

Abstract

Sandwich plates are extensively utilized across various fields, encompassing building engineering, mechanical engineering, and aerospace engineering, owing to their exceptional stiffness-to-weight ratio. However, effectively attenuating the low-frequency and broadband vibrations of these plates poses a significant challenge. This paper proposes a new type of metamaterial sandwich plate that incorporates two-degree of freedom inertial amplified resonators (IA-MSP$_{DF2}$), to attain two low-frequency band gaps (BGs) and achieve broadband vibration attenuation. The dispersion relation of the IA-MSP$_{DF2}$ is calculated based on the Bloch-Floquet theorem, and the generation mechanism of two low-frequency BGs is analyzed through eigenmodes. Both numerical and experimental studies are conducted to substantiate the advantages associated with the presence of two BGs in the IA-MSP$_{DF2}$ design. The results show that the enhanced coupling effect between the primary and secondary resonators of the IA-MSP$_{DF2}$ leads to the band associated with the local resonance that shifts to lower frequencies, resulting in a Bragg scattering BG that arises above the locally resonant BG. Compared to the metamaterial sandwich plate with one-degree of freedom inertial amplified resonators (IA-MSP$_{DF1}$) of equal mass, the IA-MSP$_{DF2}$ exhibits an increased relative bandwidth of BG by 15%. Increasing the damping of the inertial amplified resonator causes two attenuation zones to widen and merge into a wider attenuation zone. The proposed IA-MSP$_{DF2}$ can robustly and effectively attenuate the low-frequency and broadband vibration with a small mass cost, contributing to the further exploration and utilization of metamaterial sandwich plates in engineering applications.

Keywords: metamaterial sandwich plate; inertial amplification; multi-bandgap; vibration attenuation.

1. Introduction

The concept of electromagnetic metamaterials was first proposed by Veselago in 1968 [1] with extraordinary properties that are not present in nature, including negative permittivity and permeability. Owing to the mathematical similarity between acoustic and electromagnetic waves, a novel kind of metamaterials termed acoustic metamaterials (AMs) known as phononic crystals has been presented and studied recently [2-10]. AMs have attracted increasing attention due to the rich fascinating characteristics in the propagation of acoustic and vibration waves, including negative effective stiffness [11, 12], negative Poisson's ratio [13, 14], band gap (BG) [15, 16] etc. These intriguing properties have been extensively investigated for their potential to resolve acoustic and vibration problems, such as the prohibition of acoustic and vibration wave propagation within the frequency range of the BG, which presents a novel approach to vibration and noise attenuation in practical engineering.

The formation mechanisms of BGs are categorized into Bragg scattering and local resonance. AMs are composed of periodic arrangements of high-impedance scatters and a low-impedance matrix, causing the destructive Bragg scattering of the wave propagation in the structure, thus forming the Bragg scattering BG [17-19]. However, the wave wavelength corresponding to the frequency of Bragg scattering BG is of equal order as the lattice constant, thus the attenuation of low-frequency waves requires large size of the AM, which does not facilitate the practical application of AMs. To address the limitation, Liu et al. [20] proposed a new kind of AMs derived from the concept of local resonance, which were composite materials comprising rubber-coated lead spheres arranged within a resin matrix. The locally resonant BG were two orders of magnitude smaller than the incident wave wavelength, enabling a novel way to obtain low-frequency BG by small size structure. The local resonance-type

AM can be simplified the model comprising of spring-mass subsystem, which are integrated with plates, beams, and further engineering structure to exploit their low-frequency BG characteristics for sound and vibration isolation applications [21-26]. Yu et al. [21] conducted theoretical and experimental investigations to explore the vibration properties of Timoshenko beams equipped with periodically attached local resonators. The results demonstrated that the local resonators induced low-frequency bandgaps (BGs), offering a means for effectively controlling flexural vibrations in beams. Muhammad et al. [24] proposed a novel metamaterial pillared-plate structure featuring an exceptionally wide local resonance bandgap. Through numerical simulations and experimental investigations, they demonstrated that the expansion of the local resonance bandgap could be achieved by manipulating the effective mass density of the composite pillars and the stiffness of the plates. Cinefra et al. [27] conducted an analysis of elastic metamaterial plates using the Carrera Unified formulation (CUF) finite elements. The utilization of CUF finite elements resulted in improved computational efficiency for heterogeneous materials. The CUF is a versatile method that can be applied to diverse structural modeling scenarios. It is suitable for both static and dynamic analyses of the considered structures [28-33].

Sandwich plates consist of two uniform and smooth face panels and a core layer, which are essential components in various fields, such as building engineering, mechanical engineering, aerospace engineering, owing to the property of high stiffness-to-weight ratio [34-39]. However, its vibro-acoustic performance is poor especially in low-frequency ranges [40]. To ameliorate its property of the low frequency vibration attenuation, a variety of resonators (spring-mass subsystem), such as mass-beam resonators [41], plate-type resonators [42], membrane-type resonators [43], simply cantilever beam resonators [44], and other types of resonators [45-47], have been periodically incorporated into the core layer of the sandwich plate. The local resonant properties of these resonators can be activated within the BG and create inertial forces to weaken the vibration of plate [48]. Nevertheless, to achieve the low frequency BG in locally resonant-type metamaterial sandwich plate (LR-MSP), heavy resonators are typically required, resulting in a rise in the total mass of the system as well as limiting the practical applications of LR-MSPs.

An alternative method based on inertial amplification (IA) mechanism to obtain BGs without compromising the total stiffness or significantly increasing the total mass has been proposed by Yilmaz et al. [49-51]. This approach involves the creation of BGs with enhanced effective inertia by the motion amplification of small masses [52-57] and has been introduced into the design of metamaterial sandwich structures [58-61]. Xi et al. [58] developed an approach for attenuating lower-frequency vibrations using corrugated-core sandwich plates that incorporate a four-bar IA mechanism. The mechanism induces a lower-frequency BG through the creation of inertial forces at the four attachment points. Li et al. [59] proposed a metamaterial sandwich beam using lattice truss cores based on the IA mechanism to achieve broad vibration attenuation band. The results showed the broad BG by using IA mechanisms can be achieved with reduced dependency on additional mass. The authors [61] have incorporated the one-degree of freedom inertial amplified resonators into the metamaterial sandwich plate to achieve a lower-frequency vibration attenuation compared to the LR-MSP with the same mass.

Recently, multi-bandgaps mass-spring resonators have been introduced into the metamaterial plates to obtain broadband vibration attenuation [6, 62, 63]. To the best of authors' knowledge, metamaterial sandwich plates inspired by the idea of multi-bandgaps inertial amplified resonators have never been presented in the previous literature. This paper proposes a new type of metamaterial sandwich plate that incorporates two-degree of freedom inertial amplified resonators (IA-MSP$_{DF2}$) to attain two low-frequency band gaps (BGs) and achieve broadband vibration attenuation. The primary objective of this study is to analyze the effectiveness of the proposed IA-MSP$_{DF2}$ in attenuating the low-frequency vibration within the two BGs. Specifically, the study seeks: 1) to validate the location of the BGs in the dispersion relation of the IA-MSP$_{DF2}$ by both numerical analysis and experiment study; 2) to analyze the effect of damping on BGs of the IA-MSP$_{DF2}$ and explore how to widen the width of BG; 3) to quantitatively evaluate the vibration attenuation performance and lightweight design of the proposed IA-MSP$_{DF2}$ and other kinds of metamaterials sandwich plates in a normalized comparison. Therefore, in this study, the dispersion relation of the IA-MSP$_{DF2}$ is derived utilizing the Bloch-Floquet theorem to obtain BGs. The vibration transmission properties of IA-MSP$_{DF2}$ are studied based on the finite element method. An experimental specimen of IA-MSP$_{DF2}$ is fabricated and subjected to vibration transmission tests. The influence of damping on the BGs for the IA-MSP$_{DF2}$ is analyzed. Ultimately, a normalized comparison is conducted to assess the vibration attenuation performance and lightweight design of the proposed IA-MSP$_{DF2}$ and other kinds of metamaterials sandwich plates,

2. Model and method

This section mainly introduces the model of the IA-MSP$_{DF2}$ and presents the method of calculating the dispersion relation based on the Bloch-Floquet theorem. It lays foundations for subsequent numerical simulations and experimental studies.

2.1 Model description

Fig. 1(a) presents the schematic diagram of the IA-MSP$_{DF2}$. The structure consists of several bars with holes that support two face panels, and the two-degree of freedom inertial amplified resonators are periodically assembled between the face panels. Fig. 1 (b) and (c) illustrate the unit cell of IA-MSP$_{DF2}$ and its simplified unit cell model, respectively. As established in previous studies [53, 55, 61], the spring-lever-mass resonator can amplify the mass movement to increase the inertial mass of the system and achieve lower-frequency BG. The two-degree of freedom inertial amplified resonators consist of two coupled spring-lever-mass resonators. The baseplate is connected to the primary inertial amplified resonator, which is hinged with the support bar. Simultaneously, the secondary inertial amplified resonator is linked to the mass of the primary resonator and hinged with the support bar. The primary inertial amplified resonator is capable of promptly responding to the baseplate's vibration and dissipating energy by means of mass movement. Meanwhile, the secondary inertial amplified resonator can effectively scatter the vibration energy that is transferred from the mass of the primary inertial amplified resonator. The lattice constant a of IA-MSP$_{DF2}$ is 0.1 m, the face plate's thickness t is 2 mm, and other geometrical parameters of the unit cell are depicted in Fig. 2. Furthermore, l_a is 0.15a, l_b is 0.3a, l_c is 0.6a, and materials parameters of the IA-MSP$_{DF2}$ are presented in Table 1. In the numerical model, by the mesh convergence study, the supporting bar is meshed using a refined tetrahedral mesh, while the remaining parts of the structure are meshed using a refined swept mesh. The utilization of refined swept mesh in COMSOL offers notable benefits in terms of minimizing computing resource requirements, enhancing simulation efficiency, and mitigating numerical errors to ensure calculation stability. This mesh precision is determined through a mesh convergence study.

An experimental specimen of the IA-MSP$_{DF2}$ with 6 × 5 unit cells is presented in Fig. 3 (a) and (b). The spring part of the primary resonator is welded to the base panel, and the spring part of the secondary resonator is welded to the mass of the primary resonator. Both resonators are connected to the support bar by bolts. The materials and geometrical parameters of the experimental specimen are the same as those described in Table 1. The experimental setup is presented in Fig. 3 (c). A KISTLER type 9276A force hammer is used to strike the excitation point on the face panel in the *z*-direction, and a Brüel & Kjær type 4394 accelerometer is utilized to collect the acceleration at the response point. The Brüel & Kjær Pulse 3160B and Labshop are utilized for the data record and analysis.

2.2 Dispersion analysis

The dispersion relation, which is a fundamental relationship between wavenumber and frequency, characterizes the propagation behavior of waves in infinitely periodic unit cells. The frequency range without corresponding eigenvalues in the dispersion relation is referred to as the BG. In this study, the finite element method implemented in COMSOL Multiphysics 5.6 software is utilized to solve the eigenvalue for the dispersion relation of the metamaterial sandwich plate. The equations that dictate the propagation of elastic waves in the metamaterial can be formulated as follows:

$$\nabla \cdot (\boldsymbol{C} : \nabla \boldsymbol{u}(\boldsymbol{r}, \mathrm{t})) = \rho \frac{\partial^2 \boldsymbol{u}(\boldsymbol{r},t)}{\partial t^2}, \tag{1}$$

where ∇ denotes the differential operator, $\boldsymbol{C}$ and ρ denote the elasticity tensor and mass density, respectively. $\boldsymbol{u}(\boldsymbol{r}, t)$ represents the displacement vector, $\boldsymbol{r}$ represents the position vector, and t represents the time. According to the Bloch-Floquet theorem, the displacement vector is expressed as

$$\boldsymbol{u}(\boldsymbol{r}, t) = \mathrm{e}^{i(\boldsymbol{k}\cdot\boldsymbol{r}-\omega t)}\boldsymbol{u}_{\boldsymbol{k}}(\boldsymbol{r}), \tag{2}$$

where $\boldsymbol{u}_{\boldsymbol{k}}(\boldsymbol{r})$ represents the displacement modulation function, ω denotes the angular frequency, and $\boldsymbol{k}$

= ($\boldsymbol{k}_x$, $\boldsymbol{k}_y$) represents the Bloch wave vector in the Brillouin reciprocal space. The base vectors of the Brillouin reciprocal space is expressed as [64, 65]

$$\boldsymbol{k}_x = \frac{2\pi(\boldsymbol{e}_y \times \boldsymbol{e}_z)}{\boldsymbol{e}_x \cdot (\boldsymbol{e}_y \times \boldsymbol{e}_z)}; \boldsymbol{k}_y = \frac{2\pi(\boldsymbol{e}_x \times \boldsymbol{e}_z)}{\boldsymbol{e}_x \cdot (\boldsymbol{e}_y \times \boldsymbol{e}_z)}, \tag{3}$$

where $\boldsymbol{e}_x$, $\boldsymbol{e}_y$ and $\boldsymbol{e}_z$ are base vectors of the lattice vector space. Regarding the 2D metamaterial, the base vectors of the lattice space are given by

$$\boldsymbol{e}_x = (a_x, 0, 0), \boldsymbol{e}_y = (0, a_y, 0), \boldsymbol{e}_z = (0, 0, 1), \tag{4}$$

where a_x and a_y represent the lattice constants along the x- and y-direction, respectively. The direction and magnitude of the wave vector $\boldsymbol{k}$ correspond to the direction and modes of wave propagation. As a result, every point within the Brillouin zone corresponds to a wave propagation mode in an infinite structure. The modulation constant $\boldsymbol{u}_{\boldsymbol{k}}(\boldsymbol{r})$ exhibits periodicity that shares similarities with that of the lattice constant:

$$\boldsymbol{u}_{\boldsymbol{k}}(\boldsymbol{r} + \boldsymbol{a}) = \boldsymbol{u}_{\boldsymbol{k}}(\boldsymbol{r}), \tag{5}$$

where $\boldsymbol{a}$ (a_x, a_y) is the lattice vector. Substituting Eq. (5) into Eq. (2) yields the following periodic boundary condition:

$$\boldsymbol{u}(\boldsymbol{r} + \boldsymbol{a}, t) = \mathrm{e}^{i\boldsymbol{k}\cdot\boldsymbol{a}}\boldsymbol{u}(\boldsymbol{r}, t). \tag{6}$$

In the case of 2D metamaterial, the periodic boundary conditions are associated with two sets of boundary conditions along the horizontal and vertical directions, as illustrated in Fig. 4 (a).

By the combination of Eq. (1) and (6), the dispersion equation in relation to eigenvalue is procured:

$$(\boldsymbol{\Omega}(\boldsymbol{k})\text{-}\omega^2\boldsymbol{M})\cdot\boldsymbol{u} = 0, \tag{7}$$

in which $\boldsymbol{\Omega}$ and $\boldsymbol{M}$ represent the stiffness and mass matrices, respectively. By changing the wave vector

k along the boundary of the irreducible Brillouin zone (M-Γ-X-M-Y-Γ) as presented in Fig. 4 (b), the dispersion relation and eigenmodes of the unit cell can be determined. The calculation of the dispersion relation in this study is accomplished by employing characteristic frequency analysis via COMSOL Multiphysics 5.6 software.

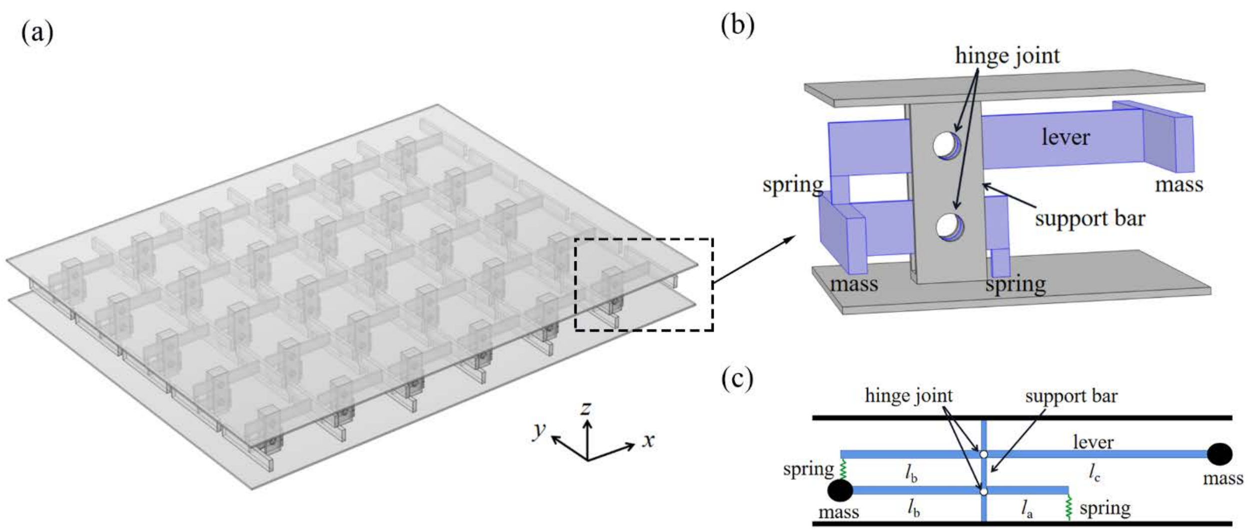

Fig. 1. The schematic diagram of the metamaterial sandwich plate with two-degree of freedom inertial amplified resonators (IA-MSP$_{DF2}$): (a) the bird's eye view of the IA-MSP$_{DF2}$; (b) the unit cell of the IA-MSP$_{DF2}$; (c) the simplified model of the unit cell for IA-MSP$_{DF2}$. (The IA-MSP$_{DF2}$ consists of several bars with holes that support two face panels, and the two-degree of freedom inertial amplified resonators are periodically assembled between the face panels. The two-degree of freedom inertial amplified resonators consist of two coupled spring-lever-mass resonators.)

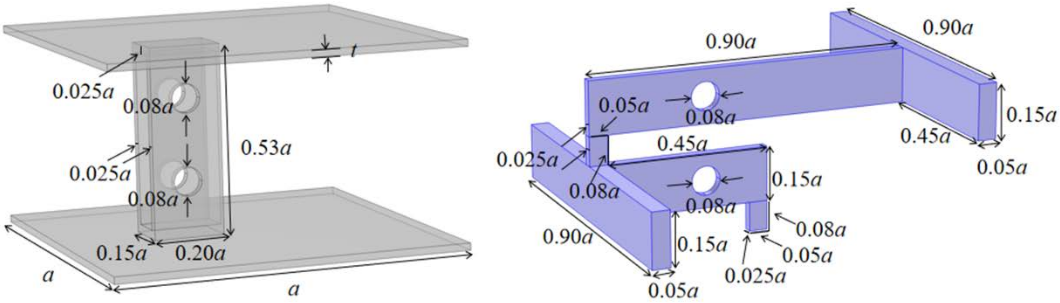

Fig. 2. The geometrical parameters of the unit cell. (The lattice constant *a* is 0.1 m; the face plate's thickness *t* is 2 mm.)

Table 1. Material parameters of the IA-MSP_{DF2}

Material	Young's modulus (GPa)	Poisson ration	Density (kg/m^3)
steel	200	0.3	7850

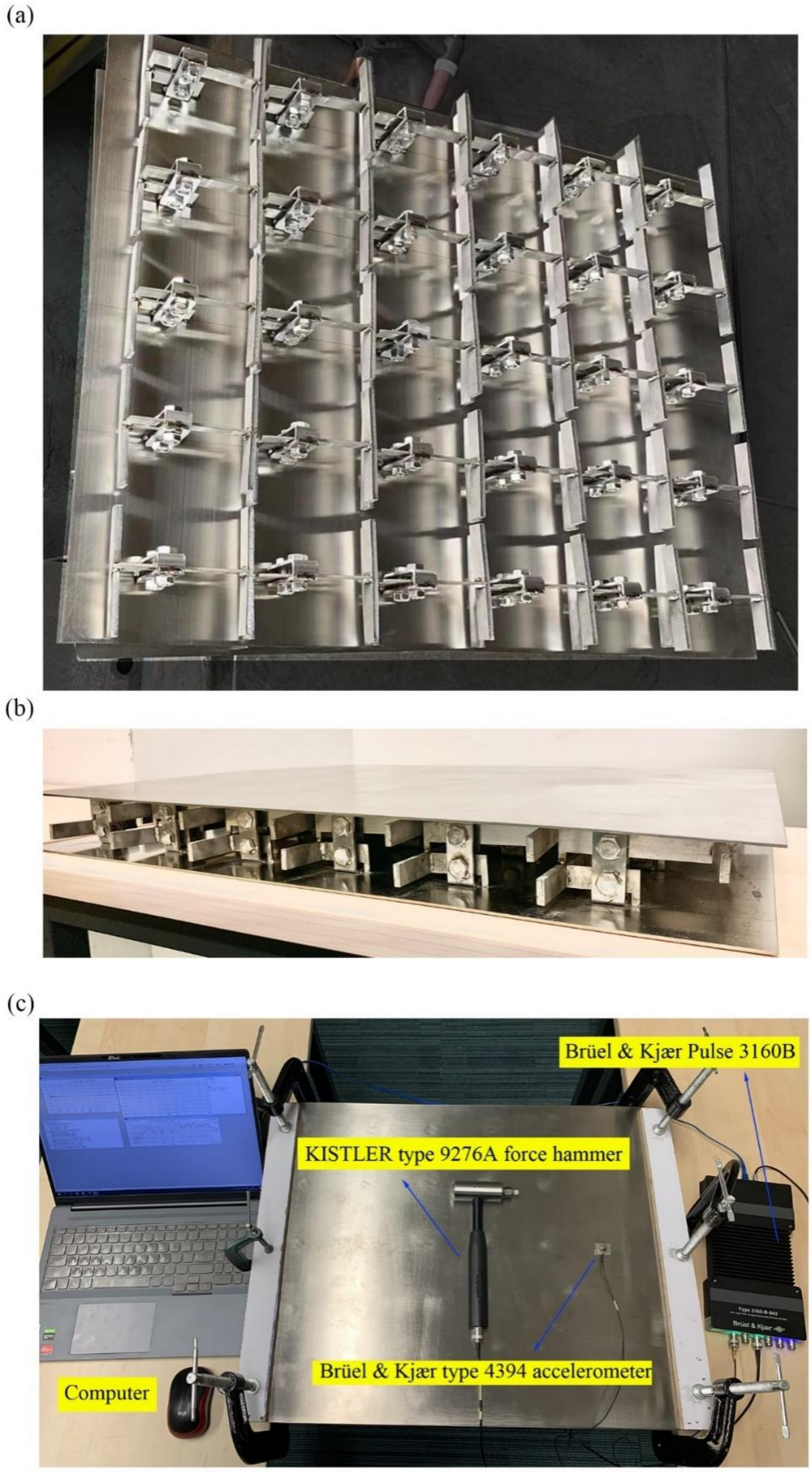

Fig. 3. The experimental specimen of the IA-MSP$_{DF2}$: (a) the experimental specimen without upper face panel; (b) the global photo of the experimental specimen; (c) the experimental setup of the vibration test.

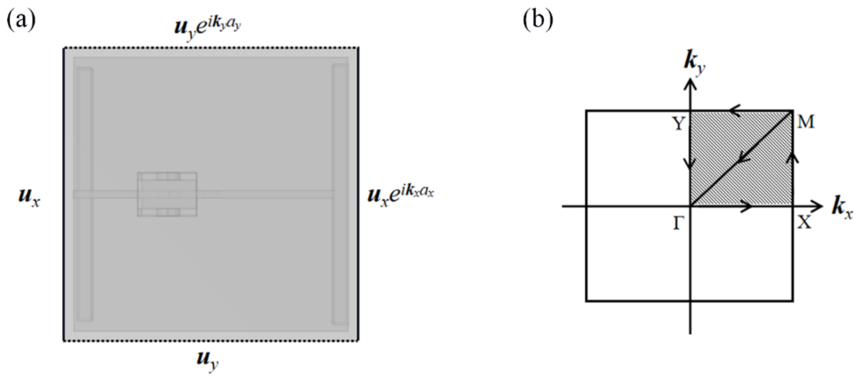

Fig. 4. (a) The periodic boundary conditions; (b) the irreducible Brillouin zone and sweeping wave vector direction (M-Γ-X-M-Y-Γ).

3. Results and discussions

This section is comprised of three main components. Firstly, the dispersion relation of the IA-MSP$_{DF2}$ is calculated, and the generation mechanism of multiple BGs is analyzed by eigenmodes. Then, the vibration properties of the IA-MSP$_{DF2}$ with 6 × 5 unit cells are investigated through numerical and experimental means. Finally, the influence of damping on the BGs is studied.

3.1 Dispersion relation of the IA-MSP$_{DF2}$

Fig. 5 (a) displays the dispersion relation of the unit cell for IA-MSP$_{DF2}$, which reveals the existence of two distinct BGs. The first band gap (BG1) spans from 511 to 628 Hz, and the second band gap (BG2) extends from 778 to 934 Hz. The eigenmode shapes (a)-(d) of the IA-MSP$_{DF2}$ correspond to the lower and upper frequency boundaries of the BG1 and BG2, respectively, as illustrated in Fig. 5 (b). The vibration deformation in eigenmode shapes (a) and (b) are primarily concentrated in the secondary inertial amplified resonator, and their vibration shapes are akin to that of eigenmode shape (e) at 599 Hz of the two-degree of freedom inertial amplified resonator. It is obvious that the acceleration integration in the *z*-direction of the eigenmode shapes (a) and (b) is non-zero, indicating that the main structure is subjected to a reaction force, which contributes to a coupling effect of the out-of-plane vibration of face panels and the resonant vibration of the inertial amplified resonator [42]. Therefore, the BG1 is the locally resonant BG. Concerning BG2, the vibration deformation of the eigenmode shapes (c) for the lower frequency boundary is concentrated in both the primary and secondary inertial amplified resonators, and it indicates that the lower boundary of BG2 is influenced by the coupling effect of the face panel vibration and the resonant vibration of the inertial amplified resonator. However, the vibration deformation of the eigenmode shapes (d) for the upper frequency boundary only appears in the face panel rather than in the resonators. Thus, the upper frequency boundary of BG2 is affected by the Bragg scattering.

To elucidate the underlying mechanism responsible for the presence of two BGs in the IA-MSP$_{DF2}$, we conduct a comparative analysis of its dispersion curve with that of the metamaterial sandwich plate with one-degree of freedom inertial amplified resonators (IA-MSP$_{DF1}$) [61]. The geometrical parameters of the unit cell for IA-MSP$_{DF1}$ are described in [61], and it shares the same material parameters as the IA-MSP$_{DF2}$, resulting in similar overall mass. Fig. 6 displays the dispersion relation of the IA-MSP$_{DF1}$ and the corresponding eigenmode shapes at the lower and upper frequency boundaries of the BG. It is evident that the IA-MSP$_{DF1}$ contains only one BG, which ranges from 486 to 682 Hz below 1200 Hz and is classified as a locally resonant BG based on the eigenmode shapes. The frequency range of BG exhibits a high degree of overlap with BG1 of the IA-MSP$_{DF2}$ due to their shared characteristic of being locally resonant BGs, which are intrinsically linked to the resonance frequency of the resonators. This near-identity in the frequency range of two BGs can be attributed to the fact that the overall masses of the resonators in both systems are equivalent. The IA-MSP$_{DF2}$ benefits from enhanced coupling between its primary and secondary resonators, which amplifies the resonance effect of the system. As a result, the L_2 band associated with local resonance shifts to lower frequencies, while the L_3 band associated with Bragg scattering remains unaffected. This shift in frequency gives rise to a new BG2, which arises between the L_2 and L_3 bands. Consequently, the design of two-degree of freedom inertial amplified resonators is more appropriate for isolating lower-frequency vibration based on multiple BGs, while simultaneously allowing for the potential to merge two BGs into a wider lower-frequency BG.

To assess the width and location of the BG, the concept of relative bandwidth (*RW*) is introduced:

$$RW = \sum_{i=1}^{n} \frac{f_{ui} - f_{li}}{0.5\left(f_{ui} + f_{li}\right)}, \tag{8}$$

where f_{ui} and f_{li} denote the upper and lower boundary frequency of the i-th BG, respectively. A higher value of the *RW* indicates that the BG is lower and wider in terms of frequency range. The *RW* for the IA-MSP$_{DF2}$ within the frequency range below 1200 Hz is 0.388, and the *RW* for the IA-MSP$_{DF1}$ within the same frequency range is 0.336. This indicates that the IA-MSP$_{DF2}$ exhibits an increased *RW* by 15% compared to the IA-MSP$_{DF1}$. To obtain a lower and wider BG, the effect of the resonator mass on BGs is analyzed. When studying the effect of one parameter, the other parameters remain constant. The r_{m1} is defined as $r_{m1} = m_1/m_a$, where m_1 denotes a varying mass of the primary inertial amplified resonator, and m_a is the initial mass of the primary inertial amplified resonator. The r_{m2} is defined as $r_{m2} = m_2/m_b$, where m_2 denotes a varying mass of the secondary inertial amplified resonator, and m_b is the initial mass of the secondary inertial amplified resonator. Fig. 7 illustrates the effect of r_{m1} and r_{m2} on the BG, while the specific result is summarized in the Table 2. It is evident that the mass of the primary inertial amplified resonator is closely related to BG2, and the lower boundary of the BG2 experiences a substantial decrease as r_{m1} increases. The two BGs tend to merge into a wider BG with increasing r_{m1}. Furthermore, the lower frequency boundary of BG1 decrease with r_{m1}, making it more likely to achieve a wider lower-frequency BG. Additionally, the mass of the secondary inertial amplified resonator is closely related to the BG1. The BG1 shifts to lower frequency with increasing r_{m2} but BG2 seems unaffected by the variation of r_{m2}. Therefore, increasing the mass of the primary inertial amplified resonator is advantageous for obtaining a wider lower-frequency BG.

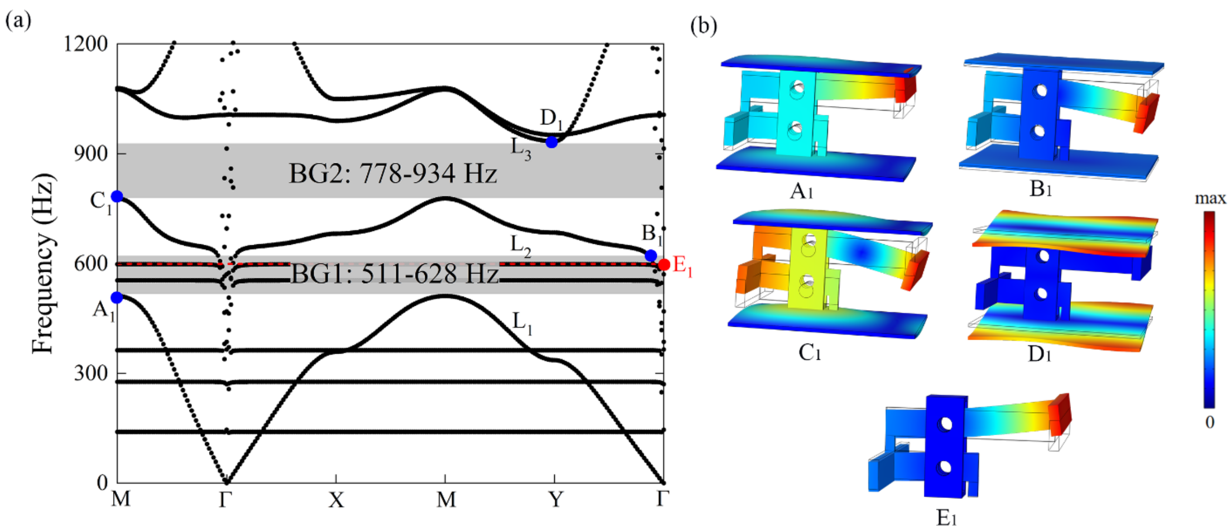

Fig. 5. Dispersion analysis. (a) Dispersion relation of the IA-MSP$_{DF2}$ (dotted black line) and eigenfrequencies of the inertial amplified resonator inducing the locally resonant BG (dashed red line); (b) eigenmode shapes (A_1, B_1, C_1, D_1) corresponding to the lower and upper frequency boundaries of the IA-MSP$_{DF2}$ and the eigenmode shape (E_1) of the two-degree of freedom inertial amplified resonator inducing the locally resonant BG. (The color bar in the visualization denotes the degree of displacement. BG1 is the first band gap, and BG2 is the second band gap.)

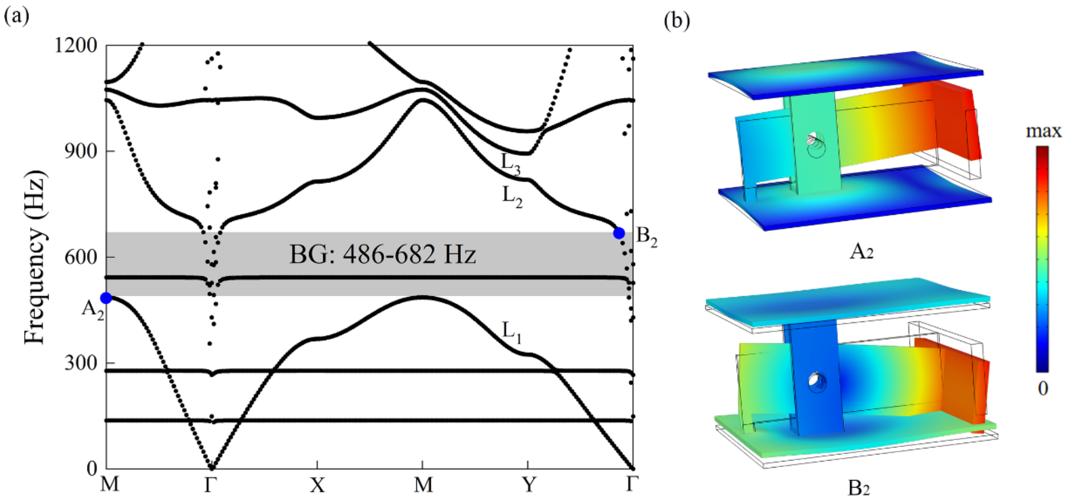

Fig. 6. Dispersion analysis. (a) Dispersion relation of the metamaterial sandwich plate with one-degree of freedom inertial amplified resonators (IA-MSP$_{DF1}$); (b) eigenmode shapes corresponding to the lower and upper frequency boundaries of the BG. (The color bar in the visualization denotes the degree of displacement.)

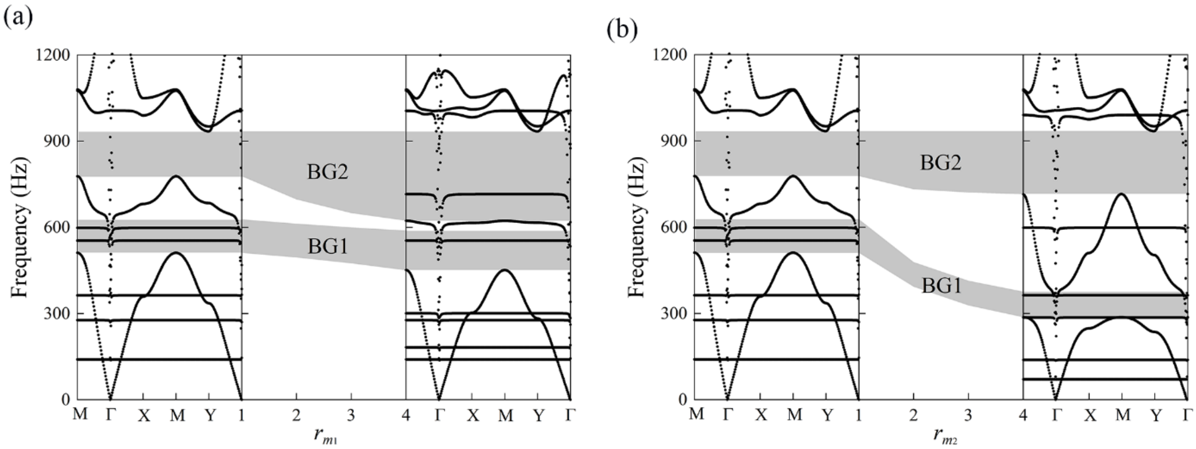

Fig. 7. The effect of r_{m1} and r_{m2} on BGs. (r_{m1} is defined as $r_{m1} = m_1/m_a$, where m_1 denotes a varying mass of the primary inertial amplified resonator, and m_a is the initial mass of the primary inertial amplified resonator. r_{m2} is defined as $r_{m2} = m_2/m_b$, where m_2 denotes a varying mass of the secondary inertial amplified resonator, and m_b is the initial mass of the secondary inertial amplified resonator.)

Table 2. The BGs and relative bandwidth (*RW*) of the IA-MSP$_{DF2}$ at different mass parameters. (r_{m1} is defined as $r_{m1} = m_1/m_a$, where m_1 denotes a varying mass of the primary inertial amplified resonator, and m_a is the initial mass of the primary inertial amplified resonator. r_{m2} is defined as $r_{m2} = m_2/m_b$, where m_2 denotes a varying mass of the secondary inertial amplified resonator, and m_b is the initial mass of the secondary inertial amplified resonator.)

Parameters (r_{m1}, r_{m2})	BG1	BG2	*RW*
1, 1	511-628 Hz	778-934 Hz	0.388
2, 1	495-613 Hz	697-934 Hz	0.504
3, 1	475-600 Hz	650-934Hz	0.591
4, 1	451-589 Hz	623-934 Hz	0.665
1, 2	393-479 Hz	732-934 Hz	0.440
1, 3	328-414 Hz	721-934 Hz	0.489
1, 4	287-376 Hz	715-934 Hz	0.534

3.2 Vibration transmission research of the IA-MSP$_{DF2}$

In practical engineering, the size of metamaterial sandwich plate is limited. Therefore, this subsection investigates the vibration transmission of the IA-MSP$_{DF2}$ with 6 × 5 unit cells to illustrate its effectiveness in isolating vibration. The model of IA-MSP$_{DF2}$ with 6 × 5 unit cells is illustrated in Fig. 8, and the materials and geometrical parameters of the unit cell are consistent with those described in Subsection 2.1. Face panels and resonators are meshed using refined swept elements, while the supporting bars are meshed using refined tetrahedral elements. Two short edges of the model are fixed boundaries, and two long edges are free boundaries. Such boundary conditions of the sandwich plates in the Ref. [41, 63]. External excitation with an amplitude of 1 N along the *z*-direction is applied at Point A (100mm, 250mm, 57mm), and the response point is at Point B (500mm, 250mm, 57mm), with a frequency interval of 5 Hz. The acceleration response of IA-MSP$_{DF2}$ with 6 × 5 unit cells is illustrated in Fig. 9. It is evident that significant amplitude attenuation occurs in two frequency ranges (grey zones), which are referred to as attenuation zone (AZ). The frequency ranges of AZ1 (510-630 Hz) and AZ2 (780-940 Hz) are almost consistent with those of BG1 and BG2 shown in Fig. 5, which confirms the results calculated by Bloch-Floquet theorem in Subsection 3.1.

To further illustrate the effectiveness of the proposed structure in attenuating vibration, the vibration modes of IA-MSP$_{DF2}$ at different excitation frequencies are calculated. Fig. 10 shows that transmitted vibration waves are almost unattenuated when the excitation frequencies are within the passband (450, 690 and 1080 Hz). However, the vibration energy within the frequency of BG (590 and 890 Hz) is centralized around the excitation point without a tendency of transmission. As seen in Fig. 10 (b), the vibration energy at 550 Hz occurs in the resonators around the excitation point, and the resonance of the inertial amplified resonator is motivated within BG1, leading to dissipation of the vibration energy. In contrast, the vibration energy at 890 Hz in Fig. 10 (d) mainly distributes in a small area of the panel near the excitation, as BG2 is caused by the periodicity of the structure rather than the resonance of the inertial amplified resonator. Additionally, the vibration transmission of IA-MSP$_{DF1}$ with 6 × 5 unit cells is studied. The condition boundaries and external excitation of the model are the same as those of the IA-MSP$_{DF2}$. The materials and geometrical parameters of the unit cell for the IA-MSP$_{DF1}$ are identical to those described in Subsection 3.1. Fig. 11 compares the acceleration response of the IA-MSP$_{DF2}$ and IA-MSP$_{DF1}$ with 6 × 5 unit cells. For the condition where the masses of two structures are almost the same, the IA-MSP$_{DF2}$ possessed two AZs below 1200 Hz compared to the IA-MSP$_{DF1}$. AZ1 (the shaded area on the left) of the IA-MSP$_{DF2}$ almost coincides with the AZ (the shaded area with oblique lines) of the IA-MSP$_{DF1}$, while the AZ2 (the shaded area on the right) occurs in a frequency region higher than the AZ1. The acceleration attenuation of the IA-MSP$_{DF2}$ in AZ1 is not significantly different from that of the IA-MSP$_{DF1}$ in AZ, but the presence of new AZ2 indicates the superiority of the multiple BG vibration attenuation. It is noted that there are some vibration attenuations in the non-bandgap range (950 Hz-1200 Hz). This phenomenon could be attributed to the fixed boundaries associated with the plate model consisting of 6 × 5 unit cells. The application of fixed boundary conditions restricts the propagation of elastic waves along the plate's edges. Therefore, elastic waves may experience reflection and interference within the plate, leading to the attenuation of vibrations at some frequencies.

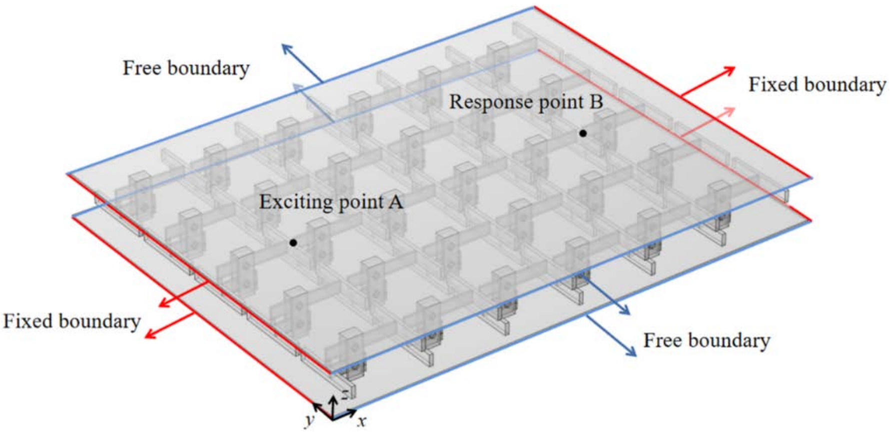

Fig. 8. The model of the IA-MSP$_{DF2}$ with 6 × 5 unit cells. (Two short red edges of the model are fixed boundaries, and two long blue edges are free boundaries.)

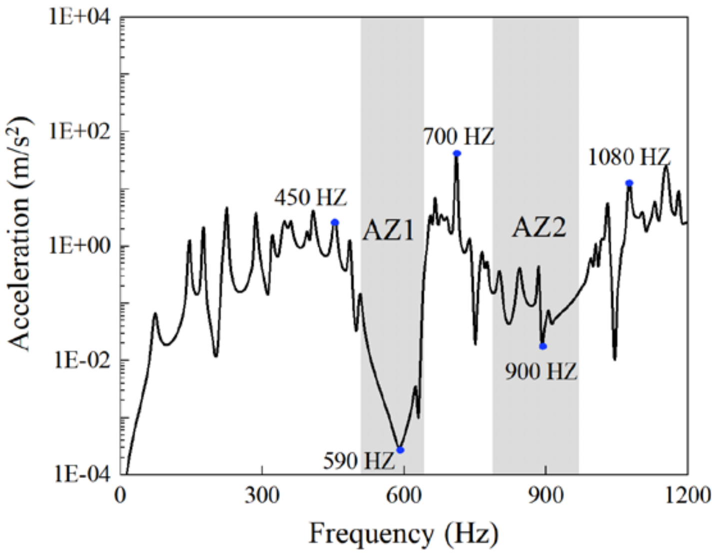

Fig. 9. The acceleration response of the IA-MSP$_{DF2}$ with 6 × 5 unit cells. (AZ1 is the first attenuation zone and AZ2 is the second attenuation zones. The frequency ranges of AZ1 (510-630 Hz) and AZ2 (780-940 Hz) are almost consistent with those of BG1 and BG2 shown in Fig. 5)

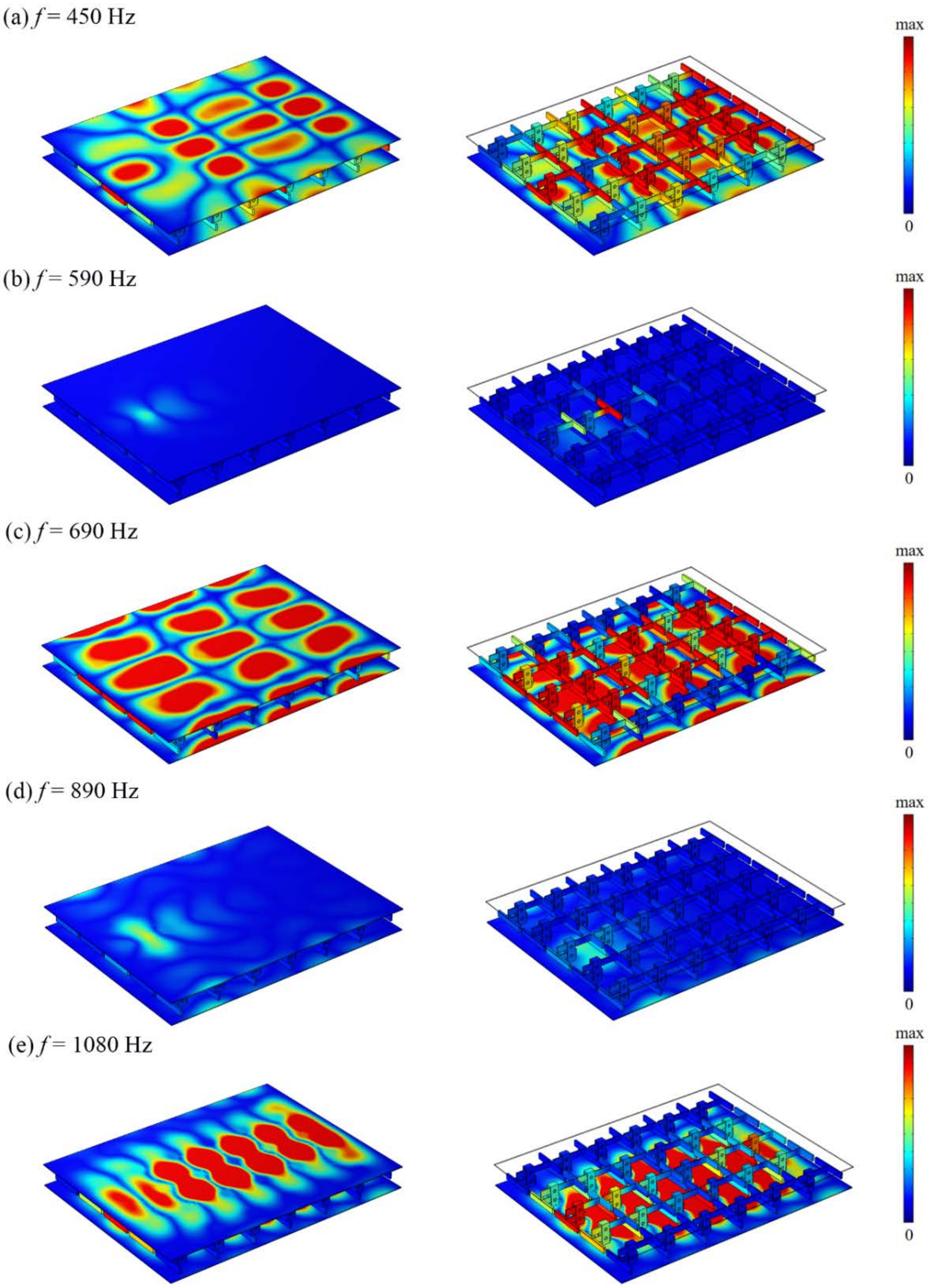

Fig. 10. Vibration modes of the faceplates and resonators of IA-MSP$_{DF2}$ at different excitation frequencies: (a) f = 450 Hz (within the passband); (b) f = 590 Hz (within the BG); (c) f = 690 Hz (within the passband); (d) f = 890 Hz (within the BG); (e) f = 1080 Hz (within the passband). The color bar in the visualization denotes the degree of displacement.

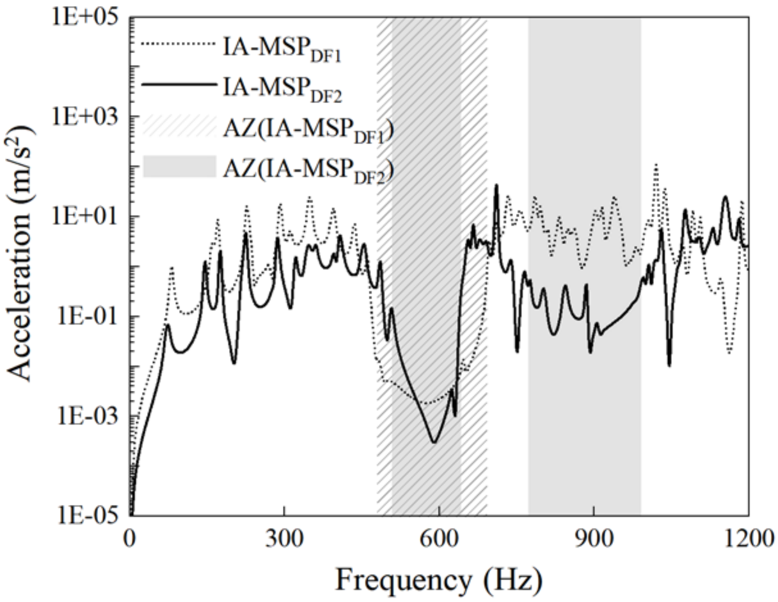

Fig. 11. The acceleration response of the IA-MSP$_{DF2}$ and IA-MSP$_{DF1}$ with 6 × 5 unit cells. (Two shaded areas are the attenuation zones (AZ) of the IA-MSP$_{DF2}$, and one shaded area with oblique lines is the AZ of the IA-MSP$_{DF1}$.

To further demonstrate the accuracy of the numerical analysis, an experimental study is conducted. The description of the experimental specimen of the IA-MSP$_{DF2}$ and the experimental setup are presented in subsection 2.1. The materials and geometrical parameters of the experimental specimen are the same as those described in the numerical study. The excitation and response points in the experiment study are consistent with those in Fig. 8. The short boundary of the specimen is fixed using clamps, while the other two long edges are free. Fig. 12 provide the dispersion relation of the IA-MSP$_{DF2}$ and acceleration response in the numerical analysis and experimental study. The dispersion relation of the IA-MSP$_{DF2}$ is calculated based on the Bloch-Floquet theorem, and the BG1 (511-628 Hz) and BG2 (778-934 Hz) are obtained shown in Fig. 12 (a). The major frequencies of attenuation band of the IA-MSP$_{DF2}$ with 6 × 5 unit cells ranges from 510 to 630 Hz and 780 to 940 Hz in the numerical analysis and experimental study shown in Fig. 12 (b) and (c). The location of AZs in the experimental study is almost consistent with that in the numerical analysis. However, the shapes of acceleration curves are not entirely identical, probably due to the experimental specimen's connection conditions and constraints not being ideal. For instance, the two short boundaries of the experimental specimen are not perfectly clamped by clamps, and the welded components are not in close contact with each other. Additionally, the discrepancy between experimental and numerical results may result from processing deviations of the specimen and material damping. Importantly, the precise control of the force magnitude applied by humans in the force hammer experiment poses challenges, thus leading to inconsistencies in the excitation magnitude between the experiment and the simulation. Therefore, different quantitative values of acceleration are observed between the numerical and experimental results. Moreover, the acceleration response curve depicted in Fig. 12 (c) from the experimental measurements exhibits more peaks in comparison to the curve presented in Fig. 12 (b) from the numerical analysis. This disparity might arise from the marginally higher stiffness of the hammer head employed in the experimental setup, resulting in an unstable initial excitation signal generated by the force hammer. The omission of various factors in the numerical simulation, such as nonlinearities, and material defects, could also contribute to this discrepancy. The presence of these factors during the experiment can exert a significant influence on the system's response, leading to the emergence of multiple peaks. Despite the discrepancy between numerical simulation results and experimental results, it has been demonstrated that the IA-MSP$_{DF2}$ is capable of isolating vibration effectively within the two BGs.

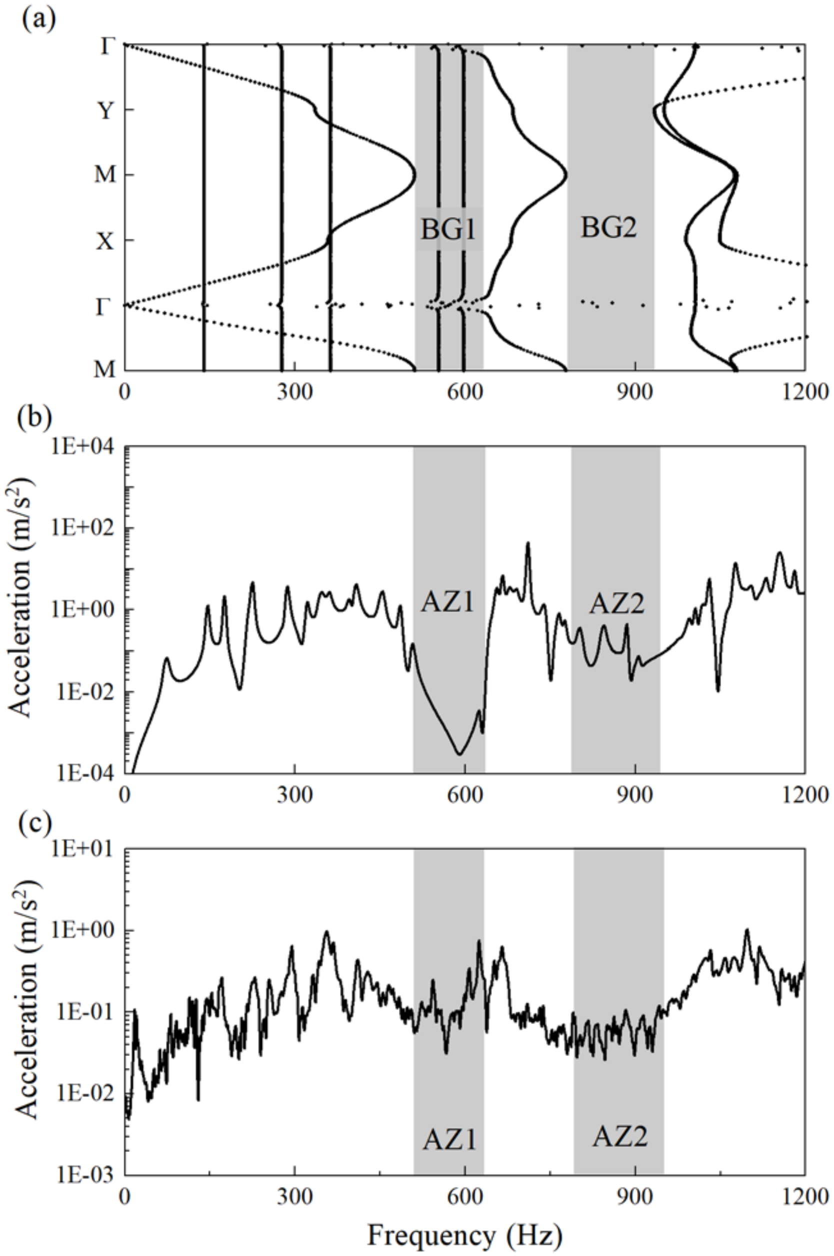

Fig. 12. The comparison of (a) the dispersion relation of the IA-MSP$_{DF2}$, (b) the acceleration response in the numerical analysis and (c) the acceleration response in the experiment study.

3.3 Effect of damping on BGs of the IA-MSP$_{DF2}$

To assess the effect of damping on BGs of the IA-MSP$_{DF2}$, the vibration response of structures is studied at different damping ratios in numerical simulation. In engineering practice, damping materials are commonly attached to resonators to vary the damping of the structure. For this numerical simulation, the damping ratio the damping ratio can be defined using complex elastic modulus $\widetilde{C} = C\,(1+\mathrm{i}\eta_s)$ of the resonator [44], where C is the elastic modulus of the resonator without damping, and η_s denotes the structural loss factor. Fig. 13 presents acceleration responses of the IA-MSP$_{DF2}$ at various damping ratios. The vibration energy in the structure is dissipated effectively due to the existence of damping. Therefore, increasing damping results in a reduction of vibration intensity and amplitude, leading to smoother response curves and the merging of the two AZs into a wider AZ. Fig. 14 illustrates vibration modes of faceplates and resonators of the IA-MSP$_{DF2}$ with $\eta_s = 0.01$ and $\eta_s = 0.2$ at different excitation frequencies. The vibration of the IA-MSP$_{DF2}$ at $\eta_s = 0.2$ attenuates significantly compared to that at $\eta_s = 0.01$ in the passband (450 and 650 Hz). It indicates the passband between BG1 and BG2 at $\eta_s = 0.2$ becomes a vibration attenuation zone. Therefore, the damping effect can merge BGs to create very wide attenuation bands, which has significant implications for the design and optimization of metamaterial structures for vibration attenuation applications.

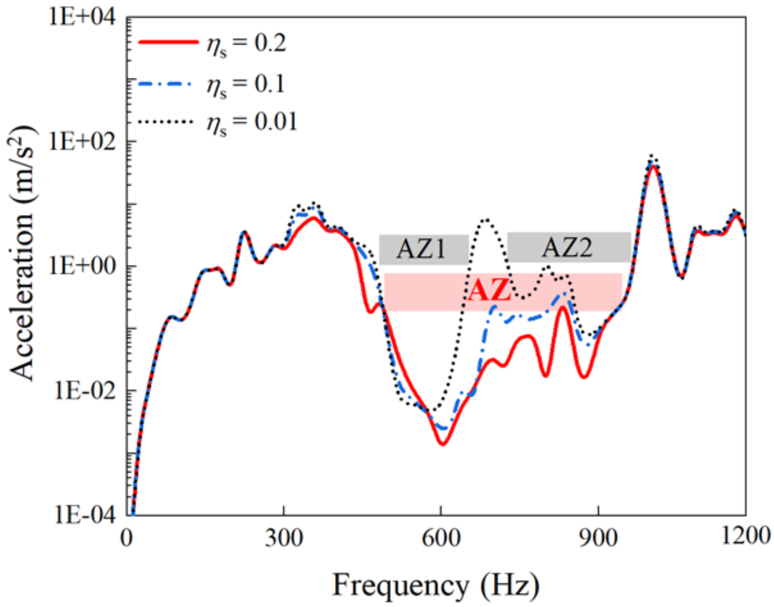

Fig. 13. The acceleration responses of IA-MSP$_{DF2}$ at different damping ratio. (η_s denotes the structural loss factor, AZ1 is the first attenuation zone at $\eta_s = 0.01$, AZ2 is the second attenuation zone at $\eta_s = 0.01$, AZ is a wide attenuation zone at $\eta_s = 0.2$).

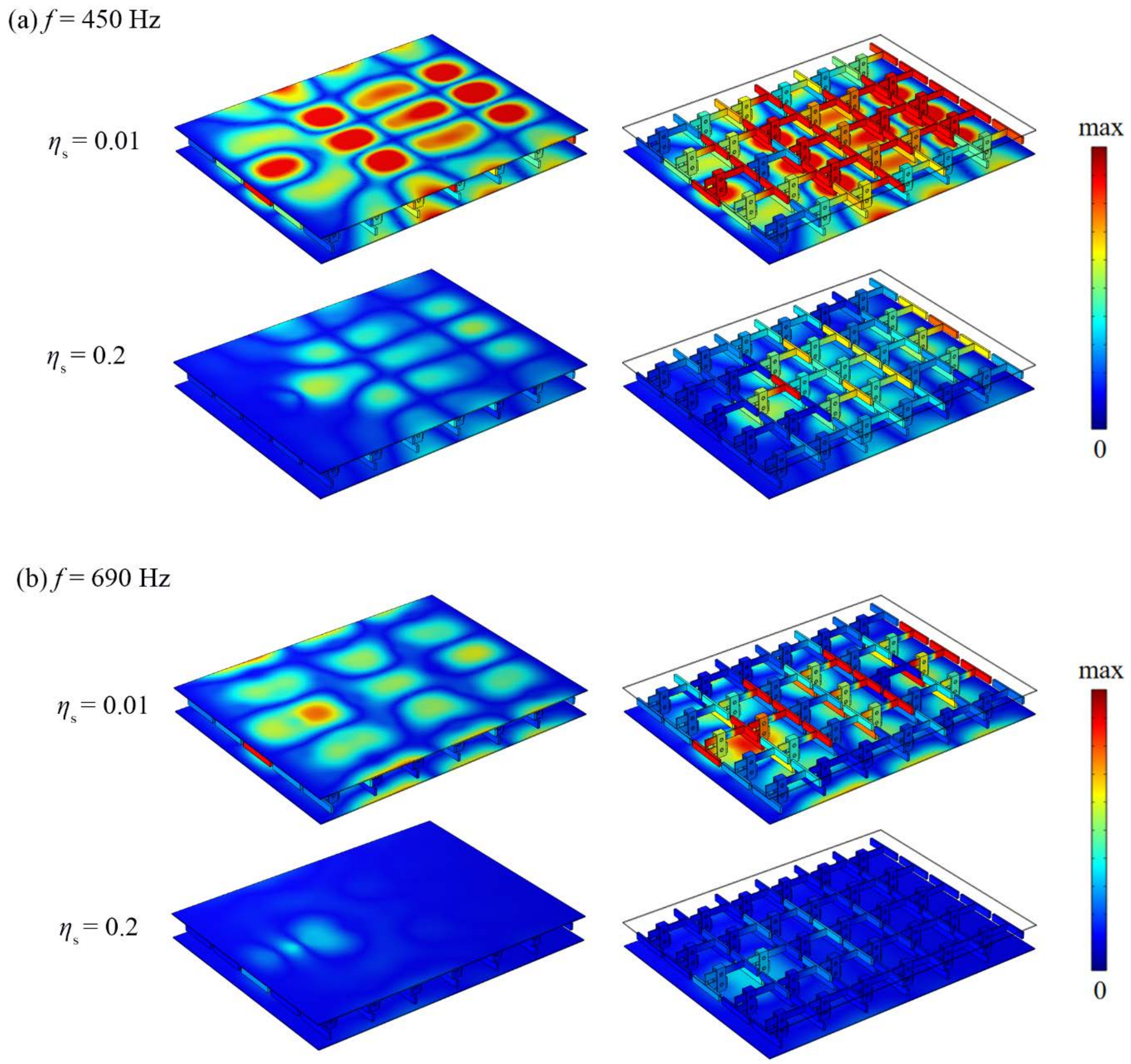

Fig. 14. Vibration modes of faceplates and resonators of IA-MSP$_{DF2}$ with $\eta_s = 0.01$ and $\eta_s = 0.2$ at different excitation frequencies: (a) $f = 450$ Hz; (b) $f = 650$ Hz. (η_s denotes the structural loss factor).

3.4 Normalized comparisons

A normalized comparison is conducted to quantitatively evaluate the vibration attenuation performance and lightweight design of the proposed structure and other kinds of metamaterials sandwich plates, as shown in Fig. 15. A normalized lower boundary frequency $f_{nd,l} = f_l a/v_s$ is introduced to evaluate quantitatively the BG characteristics [45, 66], where f_l is the lower boundary frequency of BG, a is the lattice constant, and v_s is the shear wave velocity of the host structure. A relative density $\bar{\rho}_c=\rho_c/\rho$ is used to evaluate the degree of lightweight design, which is defined as the ratio of the average density of the core ρ_c to the density of host structure material ρ [45, 67]. It is important to note that in the radar diagrams presented in Fig. 15, the coordinates of $f_{nd,l}$ and $\bar{\rho}_c$ have been taken the reciprocal to ensure a uniform representation of the performance levels. In the radar diagrams depicted in Fig. 15, it should be observed that a larger covered area in the radar diagram represents the advantageous combination of wider low-frequency vibration attenuation performance and lightweight design. Fig. 15 (a) illustrates normalized comparisons between the IA-MSP$_{DF2}$ and typical metamaterials sandwich plates. The results demonstrate that the proposed IA-MSP$_{DF2}$ exhibits the largest coverage area, indicating superior overall performance. The superiority of the IA-MSP$_{DF2}$ is clearly demonstrated when compared to both single-phase metamaterial sandwich plates (as shown in Fig. 15 (c)) and multi-phase metamaterial sandwich plates (as shown in Fig. 15 (d)). Furthermore, it showcases advantages over the IA-MSP$_{DF1}$ in terms of performance (as shown in Fig. 15 (b)). These comparisons provide further validation of the exceptional performance of the proposed IA-MSP$_{DF2}$ in terms of lightweight design, as well as its capability to achieve low-frequency and broadband vibration attenuation.

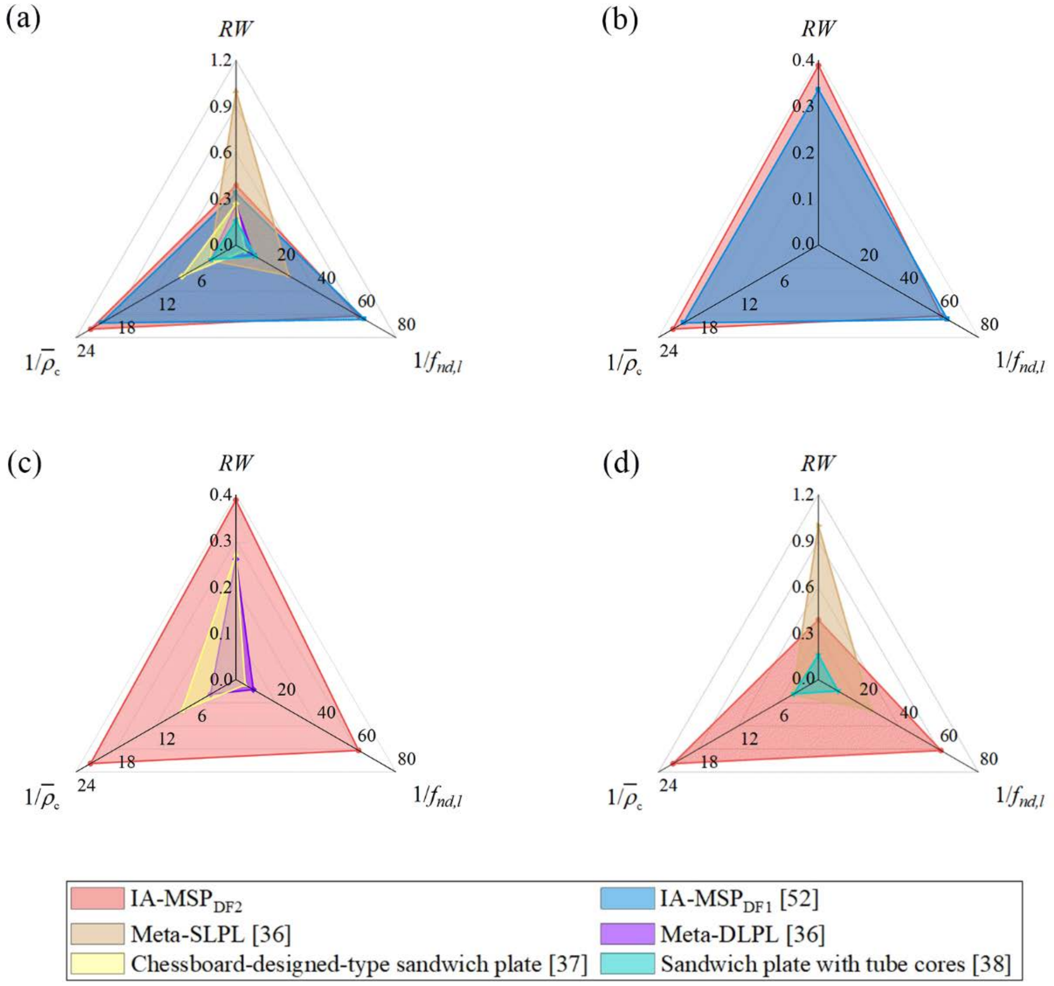

Fig. 15. Normalized comparisons in the radar diagram: (a) normalized comparisons between the IA-MSP$_{DF2}$ and typical metamaterials sandwich plates; (b) Comparison of IA-MSP$_{DF2}$ and IA-MSP$_{DF1}$; (c) IA-MSP$_{DF2}$ and single-phase metamaterials sandwich plates; (d) IA-MSP$_{DF2}$ and muti-phase metamaterials sandwich plates. (RW is the relative bandwidth of BGs. $\bar{\rho}_c$ is the relative density used to evaluate the degree of lightweight design. $f_{nd,l}$ is the normalized lower boundary frequency used to evaluate quantitatively the BG characteristics. larger covered area in the radar diagram represents the advantageous combination of wider low-frequency vibration attenuation performance and lightweight design.)

4. Conclusion

This study introduces a new type of metamaterial sandwich plate that exhibits low and multiple BGs by utilizing two-degree of freedom inertial amplified resonators to achieve broadband low-frequency vibration attenuation. Numerical analysis and experiments are conducted to analyze the vibration transmission and characteristics of IA-MSP_{DF2}. The results of the study indicate that the IA-MSP_{DF2} exhibits the presence of two BGs and a *RW* increase of 15% compared to the IA-MSP_{DF1} with an equivalent structural weight. This observed difference can be attributed to the enhanced coupling between the primary and secondary resonators of the IA-MSP_{DF2}, which amplifies the resonant effect of the system. Moreover, the lower boundary of BG2 in the IA-MSP_{DF2} exhibits a notable decrease with an increase in the mass of the primary inertial amplified resonator. As the mass of the primary resonator increases, two BGs tend to coalesce into a wider, single BG. Furthermore, increasing the damping of the inertial amplified resonator results in a decrease in vibration intensity and amplitude, which in turn leads to the merging of multiple AZs into a wider AZ. These findings provide a novel perspective on the potential of achieving a broader and lower-frequency BG for the purpose of effectively attenuating vibrations in engineering structures. The ability to broaden the BG without high attached mass in this manner opens up new possibilities for enhancing vibration control and improving the overall performance and safety of engineering systems.

Acknowledgements

This work was supported by a PhD studentship funded by Hong Kong Polytechnic University and partially supported by the National Natural Science Foundation of China (Grant No. 51908554) and Hunan Provincial Natural Science Foundation of China (Project No. 2023JJ30665).

Conflict of interest

The authors declare that they have no known competing financial interests or personal relationships that could have appeared to influence the work reported in this paper.

References

[1] V. Vesselago, "The electrodynamics of substances with simultaneously negative values of permittivity and permeability," *Sov. Phys. Usp*, vol. 10, no. 4, pp. 509-514, 1968.

[2] L. Fok, M. Ambati, and X. Zhang, "Acoustic metamaterials," *MRS bulletin*, vol. 33, no. 10, pp. 931-934, 2008.

[3] P. A. Deymier, *Acoustic metamaterials and phononic crystals*. Springer Science & Business Media, 2013.

[4] Z. He, X. Xiao, and E. Li, "Design for structural vibration suppression in laminate acoustic metamaterials," *Composites Part B: Engineering*, vol. 131, pp. 237-252, 2017.

[5] Y. Zhou, P. Wei, Y. Li, and Q. Tang, "Continuum model of acoustic metamaterials with diatomic crystal lattice," *Mechanics of Advanced Materials and Structures*, vol. 24, no. 13, pp. 1059-1073, 2017.

[6] X. Xiao, Z. He, E. Li, and A. Cheng, "Design multi-stopband laminate acoustic metamaterials for structural-acoustic coupled system," *Mechanical Systems and Signal Processing*, vol. 115, pp. 418-433, 2019.

[7] X. C. Teng *et al.*, "A simple 3D re-entrant auxetic metamaterial with enhanced energy

absorption," *International Journal of Mechanical Sciences*, vol. 229, p. 107524, 2022.

[8] H.-y. Yang *et al.*, "Multiple broadband gaps and vibration suppression mechanisms for innovative star shaped metamaterial structures with triangular characteristics," *Mechanics of Advanced Materials and Structures*, pp. 1-19, 2023.

[9] J. Li *et al.*, "Topology optimization of anisotropy hierarchical honeycomb acoustic metamaterials for extreme multi-broad band gaps," *Mechanics of Advanced Materials and Structures*, vol. 30, no. 17, pp. 3540-3552, 2023.

[10] C. Cai, Q. Xiong, L. Gao, Y. Xu, and D. Wu, "Periodic WIB-trench wave barriers for seismic surface waves," *Mechanics of Advanced Materials and Structures*, pp. 1-14, 2024.

[11] X. Zhou and G. Hu, "Analytic model of elastic metamaterials with local resonances," *Physical review. B, Condensed matter and materials physics*, vol. 79, no. 19, 2009, doi: 10.1103/PhysRevB.79.195109.

[12] S. Lin, Y. Zhang, Y. Liang, Y. Liu, C. Liu, and Z. Yang, "Bandgap characteristics and wave attenuation of metamaterials based on negative-stiffness dynamic vibration absorbers," *Journal of sound and vibration*, vol. 502, p. 116088, 2021, doi: 10.1016/j.jsv.2021.116088.

[13] H. Yasuda and J. Yang, "Reentrant origami-based metamaterials with negative Poisson's ratio and bistability," *Physical review letters*, vol. 114, no. 18, pp. 185502-185502, 2015, doi: 10.1103/PhysRevLett.114.185502.

[14] H. Chen and F. Li, "Design, simulation and experimental verification of novel 3D metamaterial structures with negative Poisson’s ratio," *Mechanics of Advanced Materials and Structures*, vol. 30, no. 1, pp. 17-28, 2023.

[15] W. Dong, T. Wang, Z. Huang, M. Chen, Q. Li, and W. Jia, "Characteristics of band gaps of a metamaterial plate with membrane-type resonators based on the energy approach," *Thin-Walled Structures,* vol. 191, p. 110930, 2023.

[16] Muhammad, C. Lim, J. Reddy, E. Carrera, X. Xu, and Z. Zhou, "Surface elastic waves whispering gallery modes based subwavelength tunable waveguide and cavity modes of the phononic crystals," *Mechanics of Advanced Materials and Structures,* vol. 27, no. 13, pp. 1053-1064, 2020.

[17] L. Brillouin, *Wave propagation in periodic structures: electric filters and crystal lattices*. Dover publications, 1953.

[18] D. M. Mead, "WAVE PROPAGATION IN CONTINUOUS PERIODIC STRUCTURES: RESEARCH CONTRIBUTIONS FROM SOUTHAMPTON, 1964–1995," *Journal of sound and vibration,* vol. 190, no. 3, pp. 495-524, 1996, doi: 10.1006/jsvi.1996.0076.

[19] S. Timorian, M. Ouisse, N. Bouhaddi, S. De Rosa, and F. Franco, "Numerical investigations and experimental measurements on the structural dynamic behaviour of quasi-periodic meta-materials," *Mechanical Systems and Signal Processing,* vol. 136, p. 106516, 2020.

[20] Z. Liu *et al.*, "Locally Resonant Sonic Materials," *Science (American Association for the Advancement of Science),* vol. 289, no. 5485, pp. 1734-1736, 2000, doi: 10.1126/science.289.5485.1734.

[21] D. Yu, Y. Liu, G. Wang, H. Zhao, and J. Qiu, "Flexural vibration band gaps in Timoshenko beams with locally resonant structures," *Journal of applied physics,* vol. 100, no. 12, p. 124901, 2006.

[22] M. Oudich *et al.*, "Experimental evidence of locally resonant sonic band gap in two-dimensional phononic stubbed plates," *Physical Review B,* vol. 84, no. 16, p. 165136, 2011.

[23] X.-W. Sun, H.-F. Zhu, X.-L. Gao, T. Song, and Z.-J. Liu, "Tunable low-frequency bandgaps of a new two-dimensional multi-component phononic crystal under different pressures, geometric parameters and pre-compression strains," *Mechanics of Advanced Materials and Structures,* vol. 29, no. 25, pp. 4019-4031, 2022.

[24] S. I. Hussain and C. Lim, "Composite trampoline metamaterial with enlarged local resonance bandgap," *Applied Acoustics,* vol. 184, p. 108353, 2021.

[25] S.-l. Cheng *et al.*, "Low frequency band gap and wave propagation mechanism of resonant hammer circular structure," *Mechanics of Advanced Materials and Structures,* pp. 1-21, 2023.

[26] C. Wang *et al.*, "Manufacturing of membrane acoustical metamaterials for low frequency noise reduction and control: a review," *Mechanics of Advanced Materials and Structures,* pp. 1-16, 2023.

[27] M. Cinefra, A. G. de Miguel, M. Filippi, C. Houriet, A. Pagani, and E. Carrera, "Homogenization and free-vibration analysis of elastic metamaterial plates by Carrera Unified Formulation finite elements," *Mechanics of Advanced Materials and Structures,* vol. 28, no. 5, pp. 476-485, 2021.

[28] E. Carrera and G. Giunta, "Refined beam theories based on a unified formulation," *International Journal of Applied Mechanics,* vol. 2, no. 01, pp. 117-143, 2010.

[29] E. Carrera, M. Filippi, and E. Zappino, "Free vibration analysis of rotating composite blades via Carrera Unified Formulation," *Composite Structures,* vol. 106, pp. 317-325, 2013.

[30] E. Carrera, M. D. Demirbas, and R. Augello, "Evaluation of stress distribution of isotropic, composite, and FG beams with different geometries in nonlinear regime via Carrera-Unified Formulation and Lagrange polynomial expansions," *Applied Sciences*, vol. 11, no. 22, p. 10627, 2021.

[31] E. Carrera and V. Zozulya, "Carrera unified formulation for the micropolar plates," *Mechanics of Advanced Materials and Structures*, vol. 29, no. 22, pp. 3163-3186, 2022.

[32] A. Pagani and E. Carrera, "Large-deflection and post-buckling analyses of laminated composite beams by Carrera Unified Formulation," *Composite Structures*, vol. 170, pp. 40-52, 2017.

[33] A. De Miguel, M. Cinefra, M. Filippi, A. Pagani, and E. Carrera, "Validation of FEM models based on Carrera Unified Formulation for the parametric characterization of composite metamaterials," *Journal of Sound and Vibration*, vol. 498, p. 115979, 2021.

[34] J. R. Vinson, "Sandwich Structures," *Applied Mechanics Reviews*, vol. 54, no. 3, pp. 201-214, 2001, doi: 10.1115/1.3097295.

[35] J. R. Vinson, "Sandwich structures: past, present, and future," *Sandwich structures*, vol. 7, pp. 3-12, 2005.

[36] M. He and W. Hu, "A study on composite honeycomb sandwich panel structure," *Materials & Design*, vol. 29, no. 3, pp. 709-713, 2008.

[37] X. C. Teng *et al.*, "Design and mechanical performance of stretchable sandwich metamaterials with auxetic panel and lattice core," *Thin-Walled Structures*, vol. 192, p. 111114, 2023.

[38] J. Chen, W. Zhang, M. Sun, M. Yao, and J. Liu, "Free vibration analysis of composite sandwich plates with different truss cores," *Mechanics of Advanced Materials and Structures*, vol. 25, no.

9, pp. 701-713, 2018.

[39] M. Hachemi, "Vibration analysis of variable stiffness laminated composite sandwich plates," *Mechanics of Advanced Materials and Structures*, vol. 27, no. 19, pp. 1687-1700, 2020.

[40] Y. Song, L. Feng, Z. Liu, J. Wen, and D. Yu, "Suppression of the vibration and sound radiation of a sandwich plate via periodic design," *International journal of mechanical sciences*, vol. 150, pp. 744-754, 2019, doi: 10.1016/j.ijmecsci.2018.10.055.

[41] J. Li, X. Fan, and F. Li, "Numerical and experimental study of a sandwich-like metamaterial plate for vibration suppression," *Composite structures*, vol. 238, p. 111969, 2020, doi: 10.1016/j.compstruct.2020.111969.

[42] Q. Wang, J. Li, Y. Zhang, Y. Xue, and F. Li, "Bandgap properties in metamaterial sandwich plate with periodically embedded plate-type resonators," *Mechanical systems and signal processing*, vol. 151, p. 107375, 2021, doi: 10.1016/j.ymssp.2020.107375.

[43] J. Li, Y. Zhang, X. Fan, and F. Li, "Multi bandgaps design of sandwich metamaterial plate with embedded membrane-type resonators," *Journal of Sandwich Structures & Materials*, vol. 25, no. 3, pp. 311-329, 2023.

[44] C. Qiang, Y. Hao, W. Zhang, J. Li, S. Yang, and Y. Cao, "Bandgaps and vibration isolation of local resonance sandwich-like plate with simply supported overhanging beam," *Applied Mathematics and Mechanics*, vol. 42, no. 11, pp. 1555-1570, 2021.

[45] H. Li, Y. Hu, H. Huang, J. Chen, M. Zhao, and B. Li, "Broadband low-frequency vibration attenuation in 3D printed composite meta-lattice sandwich structures," *Composites Part B: Engineering*, vol. 215, p. 108772, 2021.

[46] Z.-Y. Li, T.-X. Ma, Y.-Z. Wang, F.-M. Li, and C. Zhang, "Vibration isolation by novel meta-design of pyramid-core lattice sandwich structures," *Journal of Sound and Vibration,* vol. 480, p. 115377, 2020.

[47] G.-L. Yu and H.-W. Miao, "On vibration isolation of sandwich plate with periodic hollow tube core," *Journal of Sandwich Structures & Materials,* vol. 21, no. 3, pp. 1119-1132, 2019.

[48] X. An, X. Yuan, X. Hou, and H. Fan, "Low frequency vibration attenuation of meta-orthogrid sandwich panel with high load-bearing capacity," *Composite structures,* vol. 305, p. 116560, 2023, doi: 10.1016/j.compstruct.2022.116560.

[49] C. Yilmaz and N. Kikuchi, "Analysis and design of passive low-pass filter-type vibration isolators considering stiffness and mass limitations," *Journal of sound and vibration,* vol. 293, no. 1, pp. 171-195, 2006, doi: 10.1016/j.jsv.2005.09.016.

[50] C. Yilmaz, G. M. Hulbert, and N. Kikuchi, "Phononic band gaps induced by inertial amplification in periodic media," *Physical review. B, Condensed matter and materials physics,* vol. 76, no. 5, 2007, doi: 10.1103/PhysRevB.76.054309.

[51] C. Yilmaz and G. M. Hulbert, "Theory of phononic gaps induced by inertial amplification in finite structures," *Physics letters. A,* vol. 374, no. 34, pp. 3576-3584, 2010, doi: 10.1016/j.physleta.2010.07.001.

[52] M. I. Hussein, I. Patrick, A. Banerjee, and S. Adhikari, "Metadamping in inertially amplified metamaterials: Trade-off between spatial attenuation and temporal attenuation," *Journal of Sound and Vibration,* vol. 531, p. 116977, 2022.

[53] Y. Zeng *et al.*, "Seismic metamaterials: Generating low-frequency bandgaps induced by inertial

amplification," *International journal of mechanical sciences*, vol. 221, p. 107224, 2022, doi: 10.1016/j.ijmecsci.2022.107224.

[54] Y. Zeng *et al.*, "Inertially amplified seismic metamaterial with an ultra-low-frequency bandgap," *Applied Physics Letters*, vol. 121, no. 8, p. 081701, 2022.

[55] S. Wang, M. Wang, and Z. Guo, "Adjustable low-frequency bandgap of flexural wave in an Euler-Bernoulli meta-beam with inertial amplified resonators," *Physics letters. A*, vol. 417, p. 127671, 2021, doi: 10.1016/j.physleta.2021.127671.

[56] C. Xi, H. Zheng, Y. Mi, and X. Yu, "Lever-type inertial amplification plates for low-frequency vibration reduction," *Thin-Walled Structures*, vol. 192, p. 111131, 2023.

[57] D. Mu, K. Wang, H. Shu, and J. Lu, "A two-stage inertial amplification tuned mass damper with grounded stiffness element," *Mechanics of Advanced Materials and Structures*, vol. 30, no. 19, pp. 3885-3896, 2023.

[58] C. Xi, L. Dou, Y. Mi, and H. Zheng, "Inertial amplification induced band gaps in corrugated-core sandwich panels," *Composite structures*, vol. 267, p. 113918, 2021, doi: 10.1016/j.compstruct.2021.113918.

[59] J. Li, P. Yang, and S. Li, "Phononic band gaps by inertial amplification mechanisms in periodic composite sandwich beam with lattice truss cores," *Composite Structures*, vol. 231, p. 111458, 2020.

[60] J. Li, P. Yang, and M. Xia, "Actively tuning of transverse wave band gaps in hybrid sandwich beam metamaterials with shunted piezoelectric array and inertial amplification mechanism," *Journal of Intelligent Material Systems and Structures*, vol. 33, no. 20, pp. 2520-2541, 2022.

[61] L. Gao, C. M. Mak, and C. Cai, "Realizing Lower-Frequency Vibration Isolation by Metamaterial Sandwich Plate with Inertial Amplified Resonators," *Available at SSRN 4418769*.

[62] H. Peng, P. F. Pai, and H. Deng, "Acoustic multi-stopband metamaterial plates design for broadband elastic wave absorption and vibration suppression," *International journal of mechanical sciences,* vol. 103, pp. 104-114, 2015.

[63] X. Fan, J. Li, X. Zhang, and F. Li, "Multi-bandgaps metamaterial plate design using complex mass-beam resonator," *International journal of mechanical sciences,* vol. 236, p. 107742, 2022, doi: 10.1016/j.ijmecsci.2022.107742.

[64] Z. Cheng and Z. Shi, "Composite periodic foundation and its application for seismic isolation," *Earthquake Engineering & Structural Dynamics,* vol. 47, no. 4, pp. 925-944, 2018.

[65] C. Lim, "Elastic waves propagation in thin plate metamaterials and evidence of low frequency pseudo and local resonance bandgaps," *Physics Letters A,* vol. 383, no. 23, pp. 2789-2796, 2019.

[66] C. Lim, J. T. Li, and Z. Zhao, "Lightweight architected lattice phononic crystals with broadband and multiband vibration mitigation characteristics," *Extreme Mechanics Letters,* vol. 41, p. 100994, 2020.

[67] Z. Xue and J. W. Hutchinson, "A comparative study of impulse-resistant metal sandwich plates," *International Journal of Impact Engineering,* vol. 30, no. 10, pp. 1283-1305, 2004.